

RSC Advances



This is an *Accepted Manuscript*, which has been through the Royal Society of Chemistry peer review process and has been accepted for publication.

Accepted Manuscripts are published online shortly after acceptance, before technical editing, formatting and proof reading. Using this free service, authors can make their results available to the community, in citable form, before we publish the edited article. This *Accepted Manuscript* will be replaced by the edited, formatted and paginated article as soon as this is available.

You can find more information about *Accepted Manuscripts* in the [Information for Authors](#).

Please note that technical editing may introduce minor changes to the text and/or graphics, which may alter content. The journal's standard [Terms & Conditions](#) and the [Ethical guidelines](#) still apply. In no event shall the Royal Society of Chemistry be held responsible for any errors or omissions in this *Accepted Manuscript* or any consequences arising from the use of any information it contains.

Study of the hydrogen-induced amorphization in the LaNi_{2.28} alloy

Ping Li^a, Fuqiang Zhai^b, Qi Wan^a, Kuifei Zhao^a, Ziliang Li^a,

Alex A. Volinsky^c, Xuanhui Qu^{a*}

^aInstitute for Advanced Materials and Technology, University of Science and Technology Beijing, Beijing 100083, China

^bDepartament Física Aplicada, EETAC, Universitat Politècnica de Catalunya- BarcelonaTech, 08860 Castelldefels, Spain

^cDepartment of Mechanical Engineering, University of South Florida, Tampa FL 33620, USA

Abstract:

To understand the fundamental reason leading to the poor stability in LaNi_{2.28} hydrogen storage alloy, the cycling behavior of LaNi_{2.28} alloy under hydrogen has been investigated. The present study describes the hydrogen-induced amorphization (HIA) of LaNi_{2.28} alloy. The phase composition, microstructure and morphology of the phases are observed and analyzed by using X-ray diffraction and scanning electron microscopy. The crystal structure and chemical composition of the amorphized alloy are presented, and HIA is found in the sample at different hydrogenation cycle process. During the first hydrogenation cycle, the degree of HIA is indeclinable with the increased cycle. In addition, the formation processes of amorphous alloys, the occurrence of HIA and the relation between the structure of the hydrogen-induced amorphous alloy and the stability of LaNi_{2.28} are given. Some conclusions can be first summarized: $2\text{LaNi}_{2.28} + \text{H}_2 \rightarrow \text{LaNi}_{2.28}\text{H}_x$ (amorphous) + $\text{LaNi}_5\text{H}_y + \text{LaH}_2$, and the amorphous $\text{LaNi}_{2.28}\text{H}_x$ and LaNi_5H_y can desorb 50% absorption capacity, the absorption/desorption capacity is stable after the first cycle.

Keywords: Hydrogen storage alloys; LaNi_{2.28}; Transmission electron microscopy;

*Corresponding author: quxh@ustb.edu.cn (X.H Qu);

Tel: +86-10-62332700; Fax: +86-10-62334311.

Hydrogen-induced amorphization; Rare earth metals.

1. Introduction

Because of the energy crisis and environmental issue, extensive efforts have been devoted to the development of high performance hydrogen storage alloys used as the negative electrode of the nickel-metal hydride (Ni-MH) batteries in order to significantly improve the adverse effects of consumption and dependence on fossil fuels.¹⁻³ To date, the investigated hydrogen storage alloys for the negative electrode can mainly be classified into the following categories: AB₅ (CaCu₅ type), AB₃ (PuNi₃ or CeNi₃ type), A₂B₇ (Ce₂Ni₇ type), AB₂ (MgCu₂ or MgZn₂ Laves phase), AB (CsCl type), Mg-based alloys and Zr-based Laves phase alloy.⁴⁻⁷ Among them, rare earth-based AB₅-type and Zr-based Laves phase hydrogen storage alloys have been widely used in the commercial Ni-MH rechargeable battery due to their long-term cycling stability and environmental friendliness.⁸⁻¹⁰ However, with the rapid development of electronic devices requiring the Ni-MH rechargeable battery with higher overall performance, the limited discharge capacity of rare earth-based AB₅-type (300mA·hg⁻¹) and the difficult activation of Zr-based Laves phase alloy electrodes have become the main obstacles to extend their applications in the field of Ni-MH rechargeable battery.^{11,12}

It has come to light that the capacity deterioration of hydrogen storage alloy used as the negative electrode is mainly associated with pulverization, oxidation or corrosion of the alloy electrode during electrochemical charge-discharge cycling.¹³⁻¹⁵ Furthermore, it is worth to note that the hydrogen-induced amorphization (HIA) also plays a crucial role in destroying the hydrogen storage capacity and cycle stability of AB₃-type negative electrodes.¹⁶⁻¹⁹ Zhang *et al.*¹⁹ found that the AB₃-type structure consists of one-third AB₅ and two-third AB₂ subunits forming an alternating

stacking structure. For the LaNi_3 crystal structure, its LaNi_2 subunits absorb hydrogen resulting in forming an amorphous phase of LaNi_2H_x , while its LaNi_5 subunits transfer to the crystalline phase of LaNi_5H_x , which leads to crack down of the LaNi_3 crystal structure and decrease the cycle stability of the corresponding alloy. The detailed reaction process may be described as: $3\text{LaNi}_3 \rightarrow \text{LaNi}_2\text{H}_x$ (amorphous) + $\text{LaNi}_5\text{H}_y \rightarrow 3/5\text{LaH}_2 + 2/5\text{LaNi}_5\text{H}_z$. As similar with the structure of AB_3 -type alloy, A_2B_7 -type alloy consists of both half AB_5 and AB_2 subunits, while A_5B_{19} -type alloy consists of three fifth AB_5 and two fifth AB_2 subunits. It was determined that the structure stability of AB_2 subunits determines on the hydrogen storage properties of AB_3 , A_2B_7 and A_5B_{19} -type alloy. With increasing the atomic proportion of B presented element among AB_3 , A_2B_7 and A_5B_{19} -type alloy, the content of AB_2 subunits would decline resulting in improving in the cycle stability but decreasing in the theoretical hydrogen storage and electrochemical capacity. To date, the HIA has been discovered in a great numbers of intermetallics including A_3B , A_2B , AB , AB_2 , AB_3 , A_2B_7 -type alloy and so on.¹⁶⁻²³ $\text{LaNi}_{2.28}$ ($\text{La}_7\text{Ni}_{16}$) alloy contains less Ni as compared with LaNi_3 alloy, which means $\text{LaNi}_{2.28}$ alloy could be a promising candidate as the negative electrode for Ni-MH rechargeable batteries due to its high theoretical hydrogen storage capacity. Therefore, it is necessary to investigate whether $\text{LaNi}_{2.28}$ alloy exists HIA phenomenon during the absorption-desorption cycle process and the effects of HIA on the hydrogen storage capacity of $\text{LaNi}_{2.28}$ alloy if HIA exists. Unfortunately, so far the systematic investigation about HIA in $\text{LaNi}_{2.28}$ alloy have not been conducted.²⁴⁻²⁷

In order to a better understanding the underlying mechanism of why and how to avoid or lessen the HIA in $\text{LaNi}_{2.28}$ alloy for improving the cycling stability of hydrogen storage alloys as the negative electrode material, in this work, the HIA process in $\text{LaNi}_{2.28}$ alloy evolving during cycling

under hydrogen and the relationship between HIA and the microstructure of $\text{LaNi}_{2.28}$ alloy were investigated by X-ray diffraction (XRD), scanning electron microscope (SEM) coupled with energy-dispersive spectroscopy (EDS), pressure-composition-temperature (PCT) and transmission electron microscopy (TEM) measurements.

2. Experimental

Alloy ingots with nominal composition $\text{LaNi}_{2.28}$ were prepared by arc-melting the mixtures of pure La (99.9 mass%) and Ni (99.9 mass%) in a high purity argon atmosphere. To assure the homogeneity of the prepared alloy, the alloy ingots were turned over and re-melted at least three times. According to the phase diagram of La-Ni binary alloy, the annealing treatment was set at 700 °C in a bid to obtain the maximum quantity of $\text{LaNi}_{2.28}$ phases. Consequently, the alloy samples sealed inside the quartz tubes were annealed at 700 °C for 24 h in a high-purity argon atmosphere. After completing the holding time at 700 °C, the annealed quartz tubes were immediately quenched in ice water to achieve relatively larger cooling speed resulting in more the tetragonal $\text{LaNi}_{2.28}$ phases. To achieve fine powders from the annealed alloy samples, the annealed alloys were taken to conduct the mechanical ball milling by using a high-energy Spex mill (QM-3B) at the rate of 1200 rpm for 30 min. About 1.5 g of the annealed alloy sample was load into the stainless milling vial with a ball to powder weight ratio of 20:1 in a high-purity argon-filled glovebox (H_2O : <10 ppm; O_2 : <10 ppm). Consequently, the alloy samples were mechanically ground into the powders with an average 35 μm diameter. Herein, it worth to note that the steel vial should rest for 5 min after every milling 10 min during the milling process in order to prevent the temperature increasing inside the steel vial.

X-ray diffraction (XRD) measurements were performed to characterize the amorphous nature

and phase composition of as annealed $\text{LaNi}_{2.28}$ alloys by using a Rigaku D/Max diffractometer with $\text{Cu K}\alpha$ radiation ($\lambda=1.5406\times 10^{-10}$ m). The morphologies of as annealed samples were observed by using a Cambridge S360 model scanning electron microscope (SEM) coupled with energy-dispersive spectroscopy (EDS). The hydriding/dehydriding properties of the $\text{LaNi}_{2.28}$ alloy samples were measured by using a pressure-composition-temperature (PCT) apparatus (Beijing Nonferrous Metal Research Institute, China). The details of the apparatus were given in previous reports^{28,29}. Typically, 0.5 g powder sample was loaded into the vessel, and then the measuring system was pumped to a hard vacuum, then the sample was heated up to 120 °C at a 6 °C/min heating rate under 0.1 atm. Following the completion of the first absorption process, the sample was subjected to rehydrogenation at 120 °C under 3.5 MPa hydrogen pressure. Subsequently, the rehydrogenated sample was dehydrogenated at 120 °C under 0.1 MPa pressure to finish one cycle. The variation of phase composition with cycling process was examined by XRD and transmission electron microscopy (TEM).

3. Results and Discussion

3.1 Structural characteristics

Fig. 1 shows the XRD pattern of $\text{LaNi}_{2.28}$ alloy annealed at 700 °C for 24 h. As can be seen in Fig. 1, the annealed sample mainly consists of $\text{LaNi}_{2.28}$ phase but still contain little LaNi_3 second phase. In order to further prove the phase composition of the annealed $\text{LaNi}_{2.28}$ alloy, Fig. 2a exhibits the back-scattered SEM image of the annealed $\text{LaNi}_{2.28}$ alloys annealed at 700 °C for 24 h. It is obvious that the overall image is divided into two regions corresponding to grey and black region. Through EDS measurement for these two regions, it can be concluded that the grey region corresponds to $\text{LaNi}_{2.28}$ phase and the black region should be LaNi_3 , as shown in Fig. 2b and Fig. 2c.

Through analyzing the phase diagram of La-Ni alloy,³⁰ the LaNi₂ phase could be obtained by the peritectic reaction under equilibrium solidification, which means that it is difficult to obtain the single LaNi₂ phase. Moreover, Klimyenko *et al.*³¹ found that La and Ni atoms are easier to be formed into LaNi_{2.28} phase when the atomic ratio between La and Ni is 1:2, which is mainly because the atomic radius ratio between La and Ni (1.506) exists a relative greater difference with the ideal the atomic radius ratio of the Laves phase (1.225). Therefore, it is easier to be formed LaNi_{2.28} phase when the atomic ratio between La and Ni is 1:2, which can explain why more LaNi_{2.28} phases appear in Fig. 1.

3.2 Hydrogen absorption-desorption properties

Previous report on LaNi₂ found that the LaNi₂ alloy could achieve the equilibrrious compound corresponding to LaNi₂-H₂ when the LaNi₂ alloy occurs the absorption-desorption cycle.³² However, so far there is no detailed relation between absorption-desorption cycle and LaNi_{2.28} alloy. Herein, the hydrogenation properties of LaNi_{2.28} alloy were investigated to understand the effects of HIA on the hydrogenation properties of LaNi_{2.28} alloy. Fig. 3a shows the hydrogen absorption curves of the as annealed LaNi_{2.28} alloy at 120 °C under hydrogen pressure of 3.5 MPa without any activation process. As shown in Fig. 3, the as annealed LaNi_{2.28} alloy can absorb 1.6 wt.% hydrogen within 0.5 h in the above mentioned absorption condition. As compared with the traditional LaNi₃ alloy,¹⁶⁻¹⁸ the LaNi_{2.28} alloy exhibits higher hydrogen absorption behavior at relatively low temperatures (≤ 150 °C). However, the cyclic stability of LaNi_{2.28} alloy is very poor as compared with other hydrogen storage alloys. It is necessary to explore the reason for the poor cyclic stability. The desorption kinetics of LaNi_{2.28} was measured at 120 °C at an initial hydrogen pressure of 3.5 MPa without any activation process. As can be seen in Fig. 3b, the LaNi_{2.28} shows a very sluggish

hydrogen desorption kinetics. The $\text{LaNi}_{2.28}$ only desorbed about 1.0 wt. % of hydrogen at 120 °C within 1 h, indicating that the desorption kinetics of $\text{LaNi}_{2.28}$ is worse than its absorption kinetics.

Fig.4 shows the isothermal absorption-desorption curves of $\text{LaNi}_{2.28}$ alloy from the first to fourth cycle at 120 °C. Before measuring the second cycle, the sample was dehydrogenated at 120 °C for 0.5 h. It should be noted that 1.6 wt. % hydrogen remains inside the alloy sample after the first absorption process. The sloping plateau appears and the hydrogen absorption obviously decreases in the second absorption-desorption process, suggesting that the isothermal absorption-desorption curves of the second cycle is remarkably different from the first one. There is a distinct decrease of hydrogen absorption existing in absorption-desorption cycle of $\text{LaNi}_{2.28}$ alloy, indicating the formation of amorphous hydrides during the cycling process.

3.3 Structural characteristics after hydriding/dehydriding

In order to understand the change of the structure and morphology of $\text{LaNi}_{2.28}$ alloy after absorption-desorption cycles, the as-annealed alloys after hydriding/dehydriding were observed by SEM and the results are illustrated in Fig. 5. Comparing SEM images of Fig. 5 (a), (b), (c) and (d), it can be found that the change of granule sizes of the alloy samples is not obvious. This result shows that the pulverization basically occur in the process of hydriding/dehydriding, indicating that the HIA of the $\text{LaNi}_{2.28}$ alloy are main reasons leading to the efficacy loss of the alloy hydrogenation. The formation of amorphous hydrides inside of the $\text{LaNi}_{2.28}$ alloy impedes the diffusion of hydrogen atoms and decreases the dynamic property in the process of hydrogen absorption and desorption.³³ Therefore, it can be concluded that the most important approach of enhancing the cycle life of the La-Ni system ($\text{LaNi}_{2.28}$ -type) hydrogen storage electrode alloys is to improve their anti-amorphization.

Fig. 6(a) shows the XRD pattern of as-annealed alloy after the first absorption. As compared with Fig. 1, $\text{LaNi}_{2.28}$ and LaNi_3 phases disappear and the main phases are LaNi_5H_y and LaH_2 . Meanwhile, a small amount of LaNi_5 can also be observed, and the diffraction peaks are comparatively broadened. Combined with the analysis of TEM (Fig. 7), it can be observed that a few amorphous phases are formed. Moreover, the diffraction rings in SAED can be indexed with crystal planes of (111) for LaNi_5H_y , (111) for LaNi_5 and (101) for LaH_2 , which is in good agreement with XRD analysis. Fig.6 (b), (c) and (d) show the XRD patterns of alloy after first, fourth and tenth cycles, respectively. There is no diffraction peaks observed, indicating that the phases exist in the form of amorphous state. Combined with the TEM analysis (Fig. 7 (b, c, and d)), it can be concluded that the major phases are amorphous state, and minor crystal phases corresponding to LaNi_5 and LaH_2 can be seen, which is verified by SAED analysis.

It can be seen from Fig. 6 (a) and Fig. 7(a) that only partial amorphous phases can be found after absorption. The disproportionation reaction happened between $\text{LaNi}_{2.28}$ and LaNi_3 following LaH_2 and LaNi_5 formed. The major phases exist in the form of amorphous state after the first absorption, while the minor phases are LaH_2 and LaNi_5 crystalline phases, which is contradictory that LaH_2 and LaNi_5 are in amorphous state after desorption. So far this phenomenon has not been found in other literatures. Meanwhile, this phenomenon is not accord with the process of HIA, and it can be related with the process of preparing samples. The first absorption was done at 120 °C under 3.5 MPa hydrogen pressure, the XRD and TEM measurements were done after the sample cooled in electric furnace from 120 °C to room temperature, that is to say, the sample was in amorphous state after the first absorption, but the crystallization process for samples results from cooling in the electric furnace. For the samples after the first cycle, the XRD measurement was

done after the sample cooled in air from 120 °C to room temperature. It can be seen from Fig. 4 and Fig. 5, the absorption capacity is about 1.6 wt% for the first absorption, but the desorption capacity is only 0.8 wt% for the first desorption, which indicates that disproportionation reaction happens during the absorption process following LaH_2 and LaNi_5H_6 formed according to the reaction formula (1). As a support for above, the precipitation of LaH_2 and LaNi_5H_z from LaNi_2H_x is indeed observed by Chung and Lee.³⁴ According to Fig. 7, after first, fourth and tenth cycles at 120 °C, the SADP of LaNi_5 is pronounced. LaH_2 is very stable and can not desorb hydrogen at 120 °C, resulting in the decrease of desorption capacity. According to the reaction formula (1), if all $\text{La}_7\text{Ni}_{16}$ ($\text{LaNi}_{2.28}$) participates in the disproportionation reaction, the desorption capacity of the formed LaNi_5H_6 is 71.6% of the total absorption capacity, but the actual desorption capacity is 50% of the total absorption capacity, which indicates that the disproportionation reaction do not happen completely. After the absorption, amorphous $\text{LaNi}_{2.28}$, LaNi_5H_6 and LaH_2 are formed as shown in the reaction formula (2). The absorption and desorption capacity are 0.8 wt% from the second to fourth cycle, indicating that the amount of LaH_2 is stable after the first cycle and the disproportionation reaction is complete during the first cycle.



4. Conclusions

In the present work, the hydrogen storage behavior of $\text{LaNi}_{2.28}$ intermetallic is systematically studied after absorption/desorption cycling under hydrogen gas, where they undergo a degree of amorphization. The hydrogen-induced amorphization (HIA) is mainly responsible for the poor reversibility of the $\text{LaNi}_{2.28}$ intermetallic. The following conclusions can be drawn:

The hydrogen-induced amorphization (HIA) is mainly responsible for the poor reversibility of the LaNi_{2.28} alloy. The HIA mainly occurs after the first cycle. With the increase of the number of cycles, the degree of HIA is not intensified. For the LaNi_{2.28} alloy, the hydrogen absorption-desorption of its LaNi_{2.28} phase induces the local lattice to become a disorderly one, leading to the amorphous phase formation. At the same time, the LaNi₅H_x crystallites formed by the LaNi₅ subunit start to precipitate. Combining these with the XRD results in Fig. 6, it describes what happened in the LaNi_{2.28} alloy: after the first absorption, amorphous LaNi_{2.28}H_x formed, and it formed LaNi₅H_y and LaH₂ by the disproportionation reaction, amorphous LaNi_{2.28}H_x and LaNi₅H_y can desorb 50% absorption capacity, the absorption/desorption capacity is stable after the first cycle.

Acknowledgments

This work is supported by the National High-Tech R&D Program (863 Program) of China (2011AA03A408) for financial support, and the National Key Laboratory of New Metal (Z2011-11). Fuqiang Zhai thanks China Scholarship Council (CSC) for providing the scholarship.

References

- [1] H. Reardon, J. M. Hanlon, R. W. Hughes, A. Godula-Jopek, T. K. Mandal and D. H. Gregory, *Energy Environ. Sci.*, 2012, **5**, 5951-5979.
- [2] Y. B. Tan and X. B. Yu, *RSC Adv.*, 2013, **3**, 23879-23894.
- [3] X. D. Kang, K. K. Wang, Y. J. Zhong, B. Yang and P. Wang, *Phys. Chem. Chem. Phys.*, 2013, **15**, 2153-2158.
- [4] Z. Rogulski, J. Dłubakb, M. Karwowska, M. Krebs, E. Pytlik, M. Schmalz, A. Gumkowska and A. Czerwiński, *J. Power Sources*, 2010, **195**, 7517-7523.
- [5] X. Y. Zhao, L. Q. Ma, Y. Yao, Y. Ding and X. D. Shen, *Energy Environ. Sci.*, 2010, **3**, 1316-1321.
- [6] Y. F. Liu, H. G. Pan, M. X. Gao and Q. D. Wang, *J. Mater. Chem.*, 2011, **21**, 4743-4755.
- [7] K. Young, J. Nei, B. Huang and M. A. Fetcenko, *Int. J. Hydrogen Energy*, 2011, **36**, 11146-11154.

- [8] F. Feng, M. Geng and D. O. Northwood, *Int. J. Hydrogen Energy*, 2001, **7**, 725-734.
- [9] T. Kohno, H. Yoshida, F. Kawashima, T. Inaba, I. Sakai, M. Yamamoto and M. Kanda, *J. Alloys Compd.*, 2000, **311**, 5-7.
- [10] C. Khaldi, S. Boussami, R. B. Ben, H. Mathlouthi and J. Lamloumi, *Mater. Sci. Eng. B*, 2010, **175**, 22-28.
- [11] S. K. Pandey, A. Srivastava and O. N. Srivastava, *Int. J. Hydrogen Energy*, 2007, **32**, 2461-2465.
- [12] K. Young, T. Ouchi, B. Reichman, J. Koch and M. A. Fetcenko, *J. Alloys Compd.*, 2011, **509**, 7611-7617.
- [13] X. Y. Zhao, J. J. Li, Y. Yao, L. Q. Ma and X. D. Shen, *RSC Adv.*, 2012, **2**, 2149-2153.
- [14] M. F. Wen, C. L. Song, L. Chen and Y. C. Zhai, *J. Mater. Chem.*, 2002, **12**, 2543-2545.
- [15] X. Y. Zhao, L. Q. Ma and X. D. Shen, *J. Mater. Chem.*, 2012, **22**, 277-285.
- [16] W. Wang, Y. G. Chen, M. D. Tao and C. L. Wu, *J. Rare Earth.*, 2010, **28**, 443-446.
- [17] J. Chen, H. T. Takeshita, H. Tanaka, N. Kuriyama, T. Sakai, I. Uehara and M. Haruta, *J. Alloys Compd.*, 2000, **302**, 304-313.
- [18] J. Zhang, F. Fang, S. Y. Zheng, J. Zhu, G. R. Chen, D. L. Sun, M. Latroche and A. Percheron-Guegan, *J. Power Sources*, 2007, **172**, 446-450.
- [19] J. Zhang, G. Y. Zhou, G. R. Chen, M. Latroche, A. Percheron-Guegan and D. L. Sun, *Acta Mater.*, 2008, **56**, 5388-5394.
- [20] T. Kohno, H. Yoshida, F. Kawashima, T. Inaba, I. Sakai, M. Yamamoto and M. Kanda, *J. Alloys Compd.*, 2000; **311**, L5-L7.
- [21] C. Zhong, D. Chao, Y. Chen, W. Wang, D. Zhu and C. Wu, *Electrochimica Acta*, 2011, **58**, 668-673.
- [22] K. Funaki, S. Orimo and H. Fujii, *J. Alloys Compd.*, 1997, **253**, 110-113.
- [23] D. Y. Zhang, J. K. Tang and K. A. Jr Gschneidner, *J. T. Less Comm. Metal.*, 1991, **1**, 45-53.
- [24] F. L. Zhang, Y. C. Luo, Y. C. Zhang, A. Q. Deng, L. Kang and J. H. Chen, *J. T. Chinese Rare Earth Soc.*, 2006, **24**, 592-598.
- [25] Z. L. Zhou, Y. Q. Song, S. Cui, C. G. Lin and X. H. Qu, *T. Chinese J. Nonferr. Metal.*, 2007, **17**, 45-52.
- [26] L. Kang, X. G. Tian, Y. C. Luo and R. X. Yan, *J. Lanzhou Univ. Technol.*, 2008, **34**, 1-5.
- [27] I. Park, N. Terashita and E. Abe, *J. Alloys Compd.*, 2013, **580**, S81-S84.
- [28] X. P. Zheng, P. Li, I. S. Humail, F. Q. An, G. Q. Wang and X. H. Qu, *Int. J. Hydrogen Energy*, 2007, **32**, 4957-4960.
- [29] F. Q. Zhai, P. Li, A. Z. Sun, S. Wu, Q. Wan, W. N. Zhang, Y. L. Li, L. Q. Cui and X. H. Qu, *J. Phys. Chem. C*, 2012, **116**, 11939-11945.
- [30] H. J. Okamoto, *J. Phase Equil.*, 1991, **12**, 615-616.

- [31] A. V. Klimyenko, J. Seuntjens, L. L. Miller, B. J. Beaudry, R. A. Jacobson and K. A. Jr. Gschneidner, *J. Less Common Metals*, 1988, **144**, 133-141.
- [32] W. K. Hu, R. V. Denys, C. C. Nwakwuo, T. Holm, J. P. Maehlana, J. K. Solberg and V. A. Yartys, *Electrochim. Acta*, 2013, **96**, 27-33.
- [33] V. A. Yartys, O. Gutfleisch, V. V. Panasyuk and I. R. Harris, *J. Alloys Compd.*, 1997, **253-254**, 128-133.
- [34] U. I. Chung and J. Y. Lee, *J. Non-Cryst. Solids*, 1989, **110**, 203-210.

Figure captions

Fig.1 XRD pattern of LaNi_{2.28} alloy annealed at 700 °C for 24 h..

Fig.2 (a) back-scattered SEM image of the annealed LaNi_{2.28} alloys annealed at 700 °C for 24 h; Energy dispersive spectroscopy (EDS) results of (b) grey region A and (c) black region B.

Fig.3 The first hydrogen absorption-desorption curves of LaNi_{2.28} at 120 °C under a hydrogen pressure of 3.5Mpa: (a) hydrogen absorption and (b) hydrogen desorption.

Fig.4 The hydrogen capacity of pre-annealed LaNi_{2.28} alloy during 4 hydriding/dehydriding cycles at 120 °C.

Fig.5 SEM images of as-cast and hydriding/dehydriding of the microstructure: (a) as-cast; (b) 1 time hydriding/dehydriding; (c) 4 hydrogen hydriding/dehydriding cycles and (d) 10 hydriding/dehydriding cycles.

Fig.6 XRD patterns of the pre-annealed LaNi_{2.28} alloy cycled under 3.5 MPa H₂ after (a) 1 time hydrogen absorption; (b) 1 time hydrogen desorption; (c) 4 times hydrogen desorption and (d) 10 times hydrogen desorption.

Fig.7 TEM images and selected area diffraction patterns of the pre-annealed LaNi_{2.28} alloy after (a) 1 time hydrogen absorption; (b) 1 time hydrogen desorption; (c) 4 times hydrogen desorption and (d) 10 times hydrogen desorption.

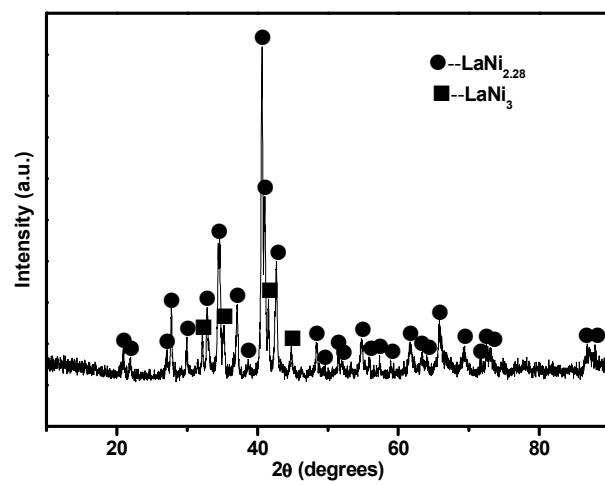


Fig.1

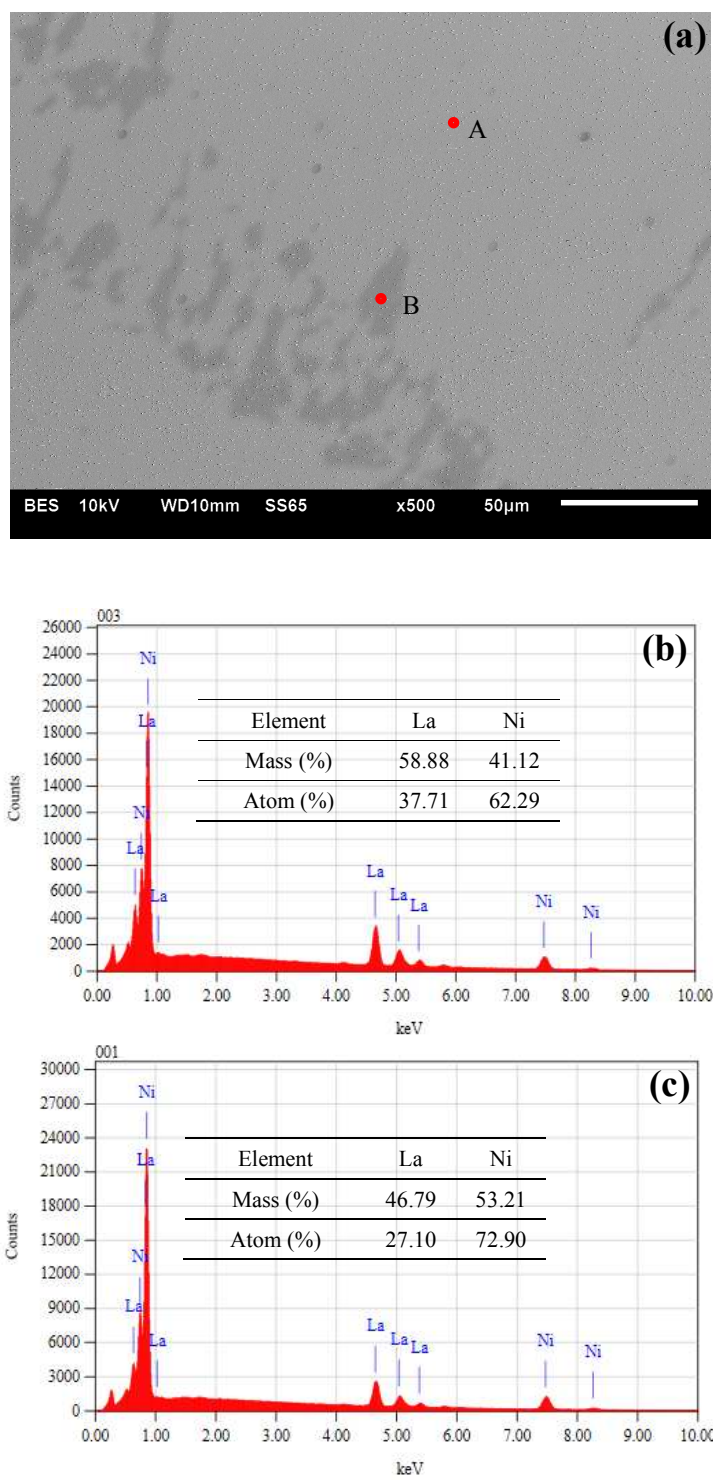


Fig.2

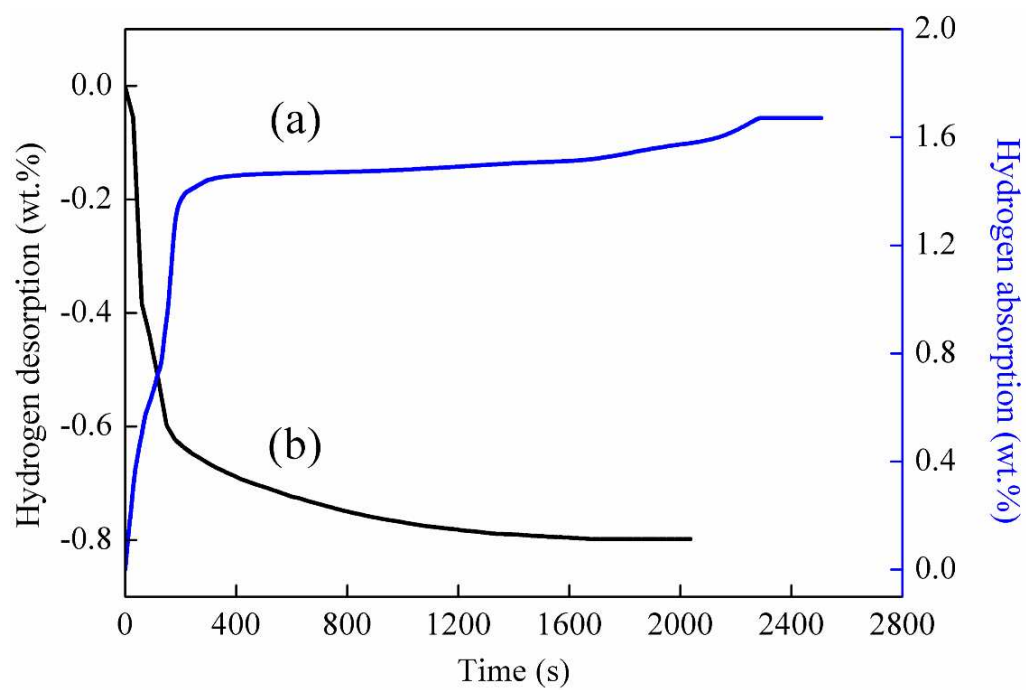


Fig. 3

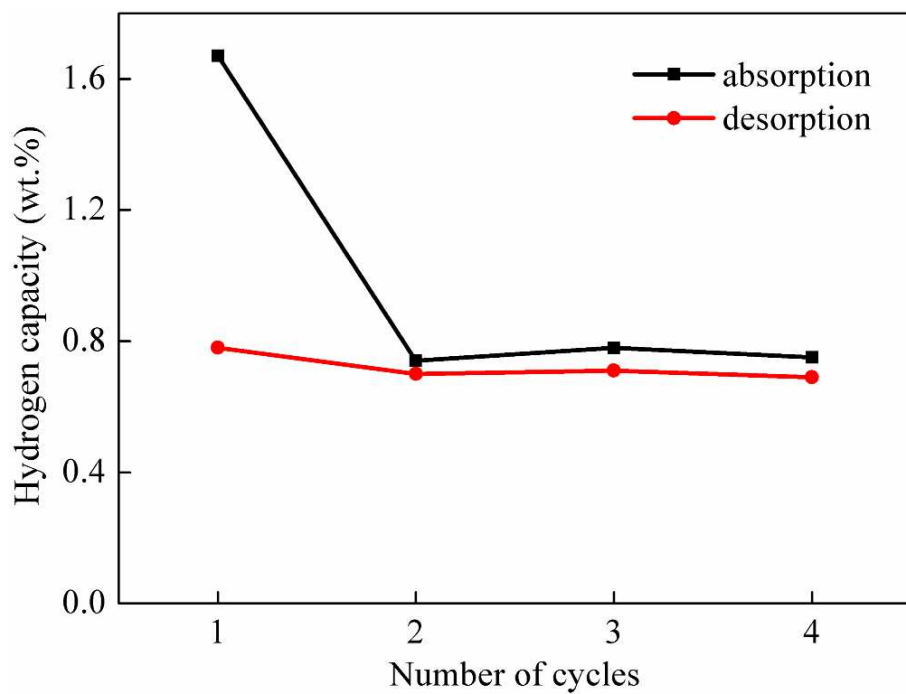
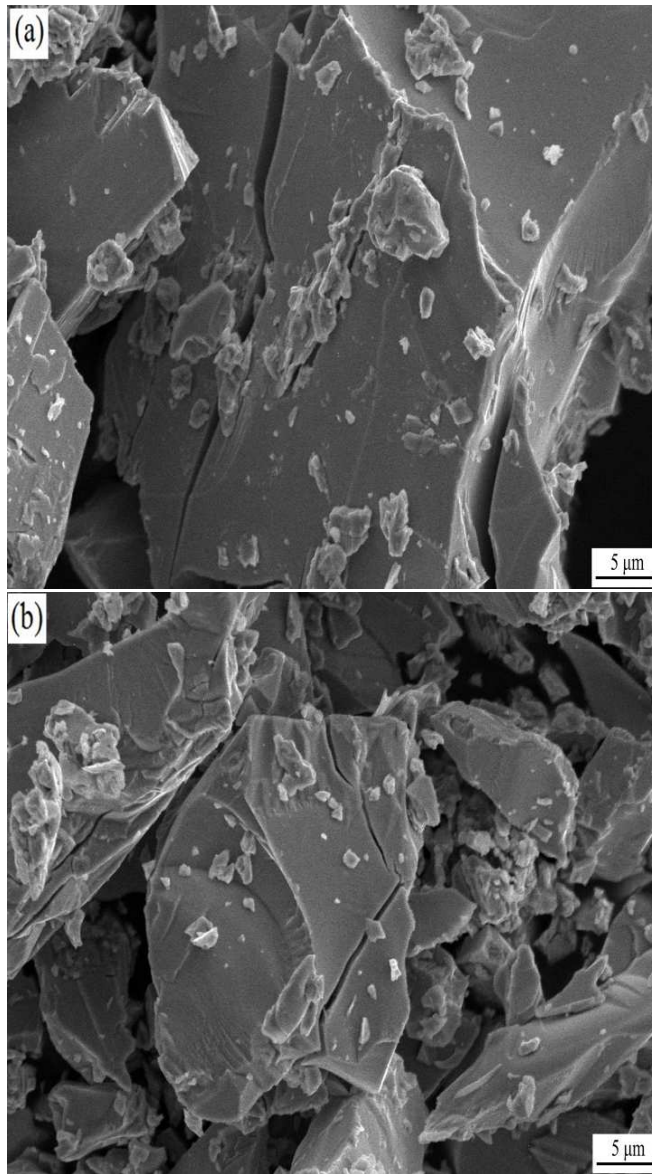


Fig. 4



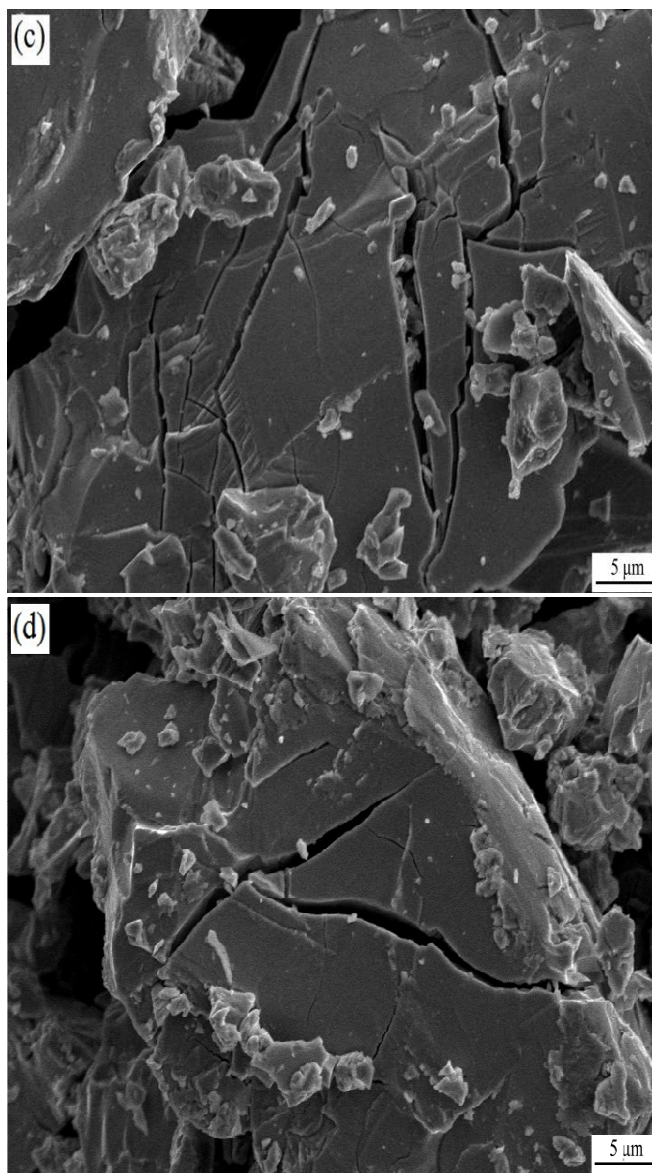


Fig. 5

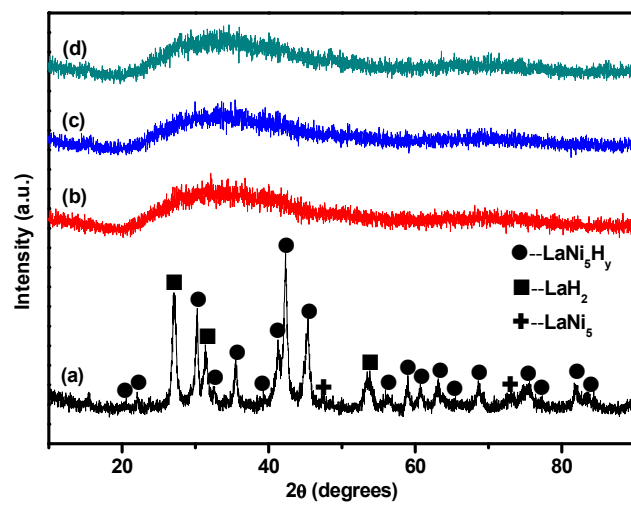
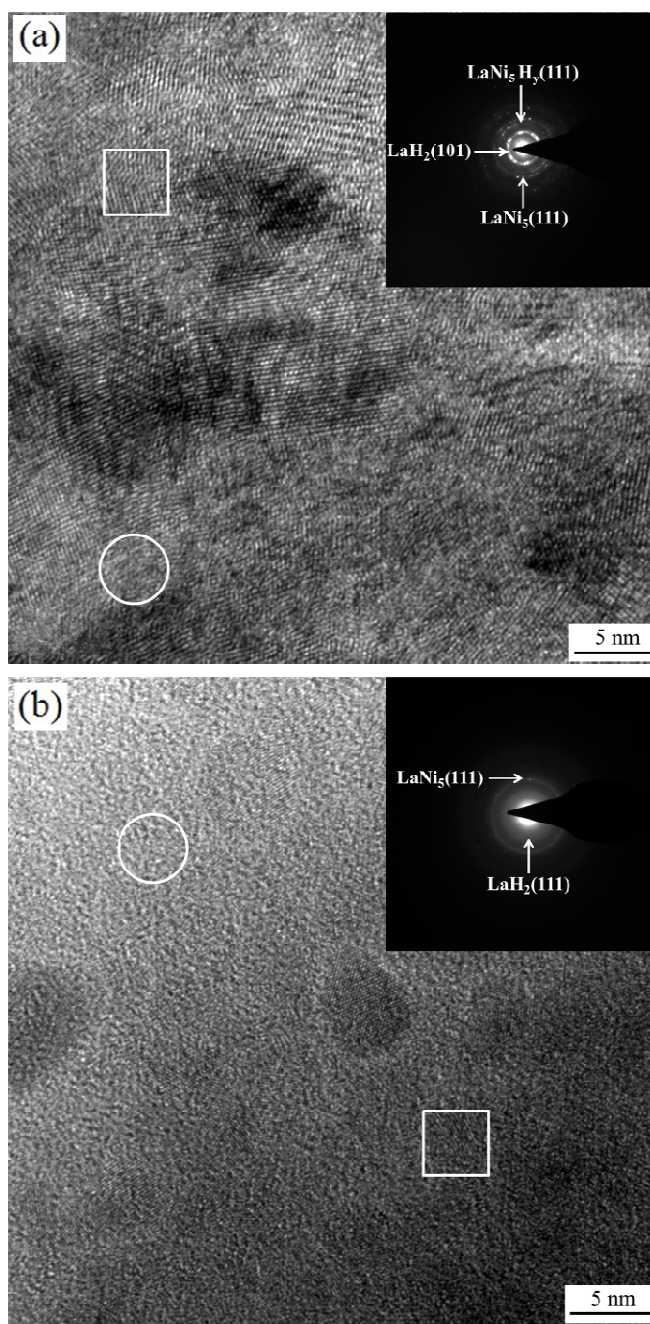


Fig. 6



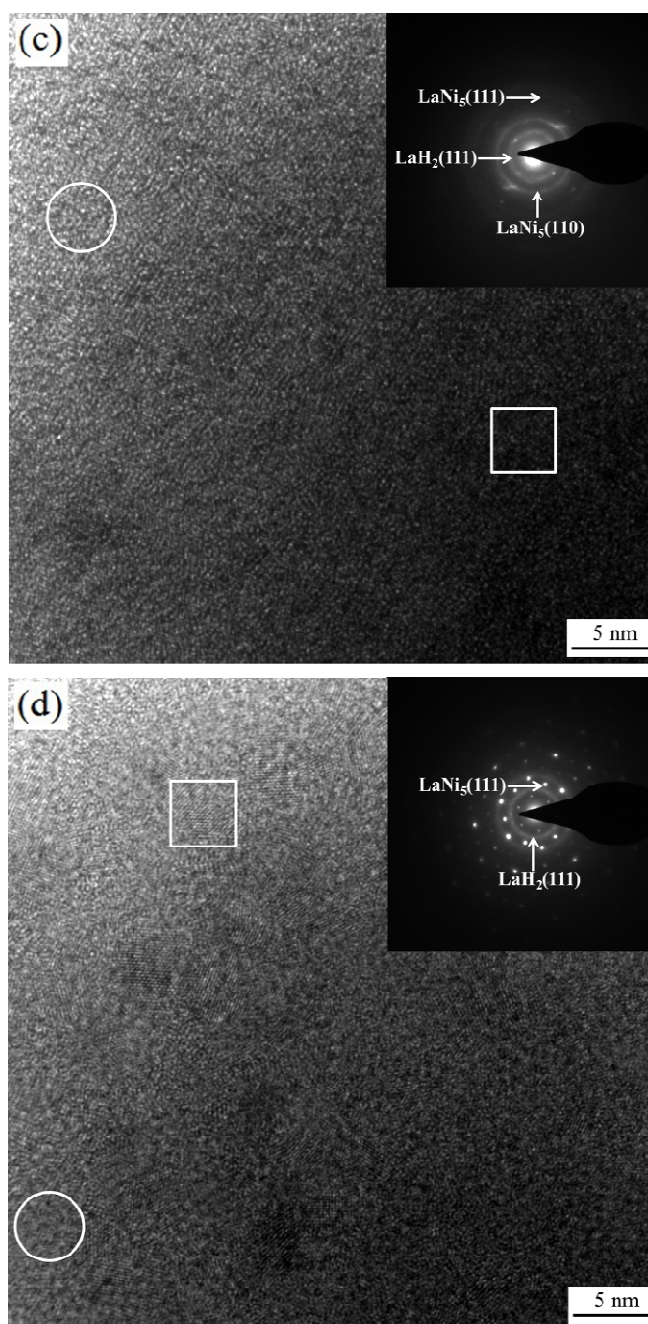


Fig. 7